

# The ASTRO-H X-ray Observatory

Tadayuki Takahashi<sup>a</sup>, Kazuhisa Mitsuda<sup>a</sup>, Richard Kelley<sup>b</sup>, Henri Aarts<sup>c</sup>,  
Felix Aharonian<sup>d</sup>, Hiroki Akamatsu<sup>c</sup>, Fumie Akimoto<sup>e</sup>, Steve Allen<sup>f</sup>, Naohisa Anabuki<sup>g</sup>,  
Lorella Angelini<sup>b</sup>, Keith Arnaud<sup>h</sup>, Makoto Asai<sup>f</sup>, Marc Audard<sup>i</sup>, Hisamitsu Awaki<sup>j</sup>,  
Philipp Azzarello<sup>i</sup>, Chris Baluta<sup>a</sup>, Aya Bamba<sup>k</sup>, Nobutaka Bando<sup>a</sup>, Mark Bautz<sup>l</sup>,  
Roger Blandford<sup>f</sup>, Kevin Boyce<sup>b</sup>, Greg Brown<sup>m</sup>, Ed Cackett<sup>n</sup>, Maria Chernyakova<sup>d</sup>,  
Paolo Coppi<sup>o</sup>, Elisa Costantini<sup>c</sup>, Jelle de Plaa<sup>c</sup>, Jan-Willem den Herder<sup>c</sup>, Michael DiPirro<sup>b</sup>,  
Chris Done<sup>p</sup>, Tadayasu Dotani<sup>a</sup>, John Doty<sup>q</sup>, Ken Ebisawa<sup>a</sup>, Megan Eckart<sup>b</sup>,  
Teruaki Enoto<sup>r</sup>, Yuichiro Ezoe<sup>s</sup>, Andrew Fabian<sup>n</sup>, Carlo Ferrigno<sup>i</sup>, Adam Foster<sup>t</sup>,  
Ryuichi Fujimoto<sup>u</sup>, Yasushi Fukazawa<sup>v</sup>, Stefan Funk<sup>f</sup>, Akihiro Furuzawa<sup>e</sup>,  
Massimiliano Galeazzi<sup>w</sup>, Luigi Gallo<sup>x</sup>, Poshak Gandhi<sup>a</sup>, Keith Gendreau<sup>b</sup>, Kirk Gilmore<sup>f</sup>,  
Daniel Haas<sup>c</sup>, Yoshito Haba<sup>e</sup>, Kenji Hamaguchi<sup>h</sup>, Isamu Hatsukade<sup>y</sup>, Takayuki Hayashi<sup>a</sup>,  
Kiyoshi Hayashida<sup>g</sup>, Junko Hiraga<sup>z</sup>, Kazuyuki Hirose<sup>a</sup>, Ann Hornschemeier<sup>b</sup>,  
Akio Hoshino<sup>u</sup>, John Hughes<sup>aa</sup>, Una Hwang<sup>ab</sup>, Ryo Iizuka<sup>ac</sup>, Yoshiyuki Inoue<sup>f</sup>,  
Kazunori Ishibashi<sup>e</sup>, Manabu Ishida<sup>a</sup>, Kosei Ishimura<sup>a</sup>, Yoshitaka Ishisaki<sup>s</sup>, Masayuki Ito<sup>ad</sup>,  
Naoko Iwata<sup>a</sup>, Naoko Iyomoto<sup>ae</sup>, Jelle Kaastra<sup>c</sup>, Timothy Kallman<sup>b</sup>, Tuneyoshi Kamae<sup>f</sup>,  
Jun Kataoka<sup>af</sup>, Satoru Katsuda<sup>r</sup>, Hajime Kawahara<sup>s</sup>, Madoka Kawaharada<sup>a</sup>,  
Nobuyuki Kawai<sup>ag</sup>, Shigeo Kawasaki<sup>a</sup>, Dmitry Khangaluyan<sup>a</sup>, Caroline Kilbourne<sup>b</sup>,  
Masashi Kimura<sup>g</sup>, Kenzo Kinugasa<sup>ah</sup>, Shunji Kitamoto<sup>ai</sup>, Tetsu Kitayama<sup>aj</sup>,  
Takayoshi Kohmura<sup>ak</sup>, Motohide Kokubun<sup>a</sup>, Tatsuro Kosaka<sup>al</sup>, Alex Koujelev<sup>am</sup>,  
Katsuji Koyama<sup>an</sup>, Hans Krimm<sup>b</sup>, Aya Kubota<sup>ao</sup>, Hideyo Kunieda<sup>e</sup>, Stephanie LaMassa<sup>o</sup>,  
Philippe Laurent<sup>ap</sup>, François Lebrun<sup>ap</sup>, Maurice Leutenegger<sup>b</sup>, Olivier Limousin<sup>ap</sup>,  
Michael Loewenstein<sup>b</sup>, Knox Long<sup>aq</sup>, David Lumb<sup>ar</sup>, Grzegorz Madejski<sup>f</sup>,  
Yoshitomo Maeda<sup>a</sup>, Kazuo Makishima<sup>z</sup>, Geneviève Marchand<sup>am</sup>, Maxim Markevitch<sup>b</sup>,  
Hironori Matsumoto<sup>e</sup>, Kyoko Matsushita<sup>as</sup>, Dan McCammon<sup>at</sup>, Brian McNamara<sup>au</sup>,  
Jon Miller<sup>av</sup>, Eric Miller<sup>l</sup>, Shin Mineshige<sup>an</sup>, Kenji Minesugi<sup>a</sup>, Ikuyuki Mitsuishi<sup>s</sup>,  
Takuya Miyazawa<sup>e</sup>, Tsunefumi Mizuno<sup>v</sup>, Hideyuki Mori<sup>a</sup>, Koji Mori<sup>y</sup>, Koji Mukai<sup>b</sup>,  
Toshio Murakami<sup>u</sup>, Hiroshi Murakami<sup>ai</sup>, Richard Mushotzky<sup>h</sup>, Housei Nagano<sup>e</sup>,  
Ryo Nagino<sup>g</sup>, Takao Nakagawa<sup>a</sup>, Hiroshi Nakajima<sup>g</sup>, Takeshi Nakamori<sup>af</sup>,  
Kazuhiro Nakazawa<sup>z</sup>, Yoshiharu Namba<sup>aw</sup>, Chikara Natsukari<sup>a</sup>, Yusuke Nishioka<sup>y</sup>,  
Masayoshi Nobukawa<sup>an</sup>, Masaharu Nomachi<sup>g</sup>, Steve O' Dell<sup>ax</sup>, Hirokazu Odaka<sup>a</sup>,  
Hiroyuki Ogawa<sup>a</sup>, Mina Ogawa<sup>a</sup>, Keiji Ogi<sup>j</sup>, Takaya Ohashi<sup>s</sup>, Masanori Ohno<sup>v</sup>,  
Masayuki Ohta<sup>a</sup>, Takashi Okajima<sup>b</sup>, Atsushi Okamoto<sup>ay</sup>, Tsuyoshi Okazaki<sup>a</sup>, Naomi Ota<sup>az</sup>,  
Masanobu Ozaki<sup>a</sup>, Frits Paerels<sup>ba</sup>, Stéphane Paltani<sup>i</sup>, Arvind Parmar<sup>bb</sup>, Robert Petre<sup>b</sup>,  
Martin Pohl<sup>i</sup>, F.Scott Porter<sup>b</sup>, Brian Ramsey<sup>ax</sup>, Rubens Reis<sup>av</sup>, Christopher Reynolds<sup>h</sup>,  
Helen Russell<sup>au</sup>, Samar Safi-Harb<sup>bc</sup>, Shin-ichiro Sakai<sup>a</sup>, Hiroaki Sameshima<sup>a</sup>,  
Jeremy Sanders<sup>n</sup>, Goro Sato<sup>a</sup>, Rie Sato<sup>a</sup>, Yoichi Sato<sup>ay</sup>, Kosuke Sato<sup>as</sup>, Makoto Sawada<sup>k</sup>,  
Peter Serlemitsos<sup>b</sup>, Hiromi Seta<sup>ai</sup>, Yasuko Shibano<sup>a</sup>, Maki Shida<sup>a</sup>, Takanobu Shimada<sup>a</sup>,  
Keisuke Shinozaki<sup>ay</sup>, Peter Shirron<sup>b</sup>, Aurora Simionescu<sup>f</sup>, Cynthia Simmons<sup>b</sup>,  
Randall Smith<sup>t</sup>, Gary Sneiderman<sup>b</sup>, Yang Soong<sup>b</sup>, Lukasz Stawarz<sup>a</sup>, Yasuharu Sugawara<sup>ac</sup>,  
Hiroyuki Sugita<sup>ay</sup>, Satoshi Sugita<sup>e</sup>, Andrew Szymkowiak<sup>o</sup>, Hiroyasu Tajima<sup>e</sup>,  
Hiromitsu Takahashi<sup>v</sup>, Shin-ichiro Takeda<sup>a</sup>, Yoh Takei<sup>a</sup>, Toru Tamagawa<sup>r</sup>,  
Takayuki Tamura<sup>a</sup>, Keisuke Tamura<sup>e</sup>, Takaaki Tanaka<sup>an</sup>, Yasuo Tanaka<sup>a</sup>,  
Makoto Tashiro<sup>bd</sup>, Yuzuru Tawara<sup>e</sup>, Yukikatsu Terada<sup>bd</sup>, Yuichi Terashima<sup>j</sup>,

Francesco Tombesi<sup>b</sup>, Hiroshi Tomida<sup>a</sup>, Yoko Tsuboi<sup>ac</sup>, Masahiro Tsujimoto<sup>a</sup>,  
Hiroshi Tsunemi<sup>g</sup>, Takeshi Tsuru<sup>an</sup>, Hiroyuki Uchida<sup>an</sup>, Yasunobu Uchiyama<sup>f</sup>,  
Hideki Uchiyama<sup>z</sup>, Yoshihiro Ueda<sup>an</sup>, Shiro Ueno<sup>ay</sup>, Shinichiro Uno<sup>be</sup>, Meg Urry<sup>o</sup>,  
Eugenio Ursino<sup>w</sup>, Cor de Vries<sup>c</sup>, Atsushi Wada<sup>ay</sup>, Shin Watanabe<sup>a</sup>, Norbert Werner<sup>f</sup>,  
Nicholas White<sup>b</sup>, Takahiro Yamada<sup>a</sup>, Shinya Yamada<sup>r</sup>, Hiroya Yamaguchi<sup>t</sup>,  
Noriko Yamasaki<sup>a</sup>, Shigeo Yamauchi<sup>az</sup>, Makoto Yamauchi<sup>y</sup>, Yoichi Yatsu<sup>ag</sup>,  
Daisuke Yonetoku<sup>u</sup>, Atsumasa Yoshida<sup>k</sup> Takayuki Yuasa<sup>a</sup>

<sup>a</sup>Institute of Space and Astronautical Science (ISAS), JAXA, Kanagawa 252-5210, Japan;

<sup>b</sup>NASA/Goddard Space Flight Center, Greenbelt, MD 20771, USA;

<sup>c</sup>SRON Netherlands Institute for Space Research, Utrecht, the Netherlands;

<sup>d</sup>Dublin Institute for Advanced Studies, Dublin, Ireland; <sup>e</sup>Department of Physics, Nagoya

University, Nagoya 338-8570, Japan; <sup>f</sup>Kavli Institute for Particle Astrophysics and

Cosmology, Stanford University, Stanford, CA 94305, USA; <sup>g</sup>Department of Earth and

Space Science, Osaka University, Osaka 560-0043, Japan; <sup>h</sup>Department of Physics,

University of Maryland, College Park, MD 21250, USA; <sup>i</sup>Université de Geneve24, Geneve,

Switzerland; <sup>j</sup>Department of Physics, Ehime University, Ehime 790-8577, Japan;

<sup>k</sup>Department of Physics and Mathematics, Aoyama Gakuin University, Kanagawa

229-8558, Japan; <sup>l</sup>Kavli Institute for Astrophysics and Space Research, Massachusetts

Institute of Technology, Cambridge, MA 02139, USA; <sup>m</sup>Lawrence Livermore National

Laboratory, Livermore CA, 94550, USA; <sup>n</sup>Institute of Astronomy, Cambridge University,

Cambridge, CB3 0HA, UK; <sup>o</sup>Department of Physics, Yale University, New Haven, CT

06520, USA; <sup>p</sup>Department of Physics, University of Durham, Durham City, DH1 3LE, UK;

<sup>q</sup>Noqi Aerospace, Pine, CO 80470, USA; <sup>r</sup>RIKEN, Saitama 351-0198, Japan; <sup>s</sup>Department

of Physics, Tokyo Metropolitan University, Tokyo 192-0397, Japan; <sup>t</sup>Harvard-Smithsonian

Center for Astrophysics, Cambridge MA 02138, USA; <sup>u</sup>Faculty of Mathematics and

Physics, Kanazawa University, Ishikawa 920-1192, Japan; <sup>v</sup>Department of Physical Science,

Hiroshima University, Hiroshima 739-8526, Japan; <sup>w</sup>Physics Department, University of

Miami, Coral Gables. FL 33124, USA; <sup>x</sup>Department of Astronomy and Physics, Saint

Mary's University, Halifax, Nova Scotia, B3H 3C3, Canada; <sup>y</sup>Department of Applied

Physics, University of Miyazaki, Miyazaki 889-2192, Japan; <sup>z</sup>Department of Physics,

University of Tokyo, Tokyo 113-0033, Japan; <sup>aa</sup>Department of Physics and Astronomy,

Rutgers University, Piscataway, NJ 08854, USA; <sup>ab</sup>Department of Physics and Astronomy,

Johns Hopkins University, Baltimore, MD 21218, USA; <sup>ac</sup>Department of Physics, Chuo

University, Tokyo 112-8551, Japan; <sup>ad</sup>Faculty of Human Development, Kobe University,

Hyogo 657-8501, Japan; <sup>ae</sup>Department of Applied Quantum Physics and Nuclear

Engineering, Fukuoka 819-0395 Japan; <sup>af</sup>Research Institute for Science and Engineering,

Waseda University, Tokyo 169-8555, Japan; <sup>ag</sup>Department of Physics, Tokyo Institute of

Technology, Tokyo 152-8551, Japan; <sup>ah</sup>Gunma Astronomical Observatory, Gunma

377-0702, Japan; <sup>ai</sup>Department of Physics, Rikkyo University, Tokyo 171-8501, Japan;

<sup>aj</sup>Department of Physics, Toho University, Chiba 274-8510, Japan; <sup>ak</sup>Department of

Physics, Kougakuin University, Tokyo 192-0015, Japan; <sup>al</sup>School of Systems Engineering,

Kochi University of Technology, Kochi 782-8502, Japan; <sup>am</sup>Space Exploration Development

Space Exploration, Canadian Space Agency, Saint-Hubert QC J3Y 8Y9, Canada;

<sup>an</sup>Department of Physics and Department of Astronomy, Kyoto University, Kyoto 606-8502,

Japan; <sup>ao</sup>Department of Electronic Information Systems, Shibaura Institute of Technology,

Saitama 337-8570, Japan; <sup>ap</sup>IRFU/Service d’Astrophysique, CEA Saclay, France; <sup>aq</sup>Space Science Telescope Institute, Baltimore, MD 21218 USA; <sup>ar</sup>ESTEC, Noordwijk, The Netherlands; <sup>as</sup>Department of Physics, Tokyo University of Science, Tokyo 162-8601, Japan; <sup>at</sup>Department of Physics, University of Wisconsin, Madison, WI 53706, USA; <sup>au</sup>University of Waterloo, Waterloo, Ontario, N2L 3G1, Canada; <sup>av</sup>Department of Astronomy, University of Michigan, Ann Arbor, MI 48109, USA; <sup>aw</sup>Department of Mechanical Engineering, Chubu University, Aichi 487-8501, Japan; <sup>ax</sup>NASA/Marshall Space Flight Center, Huntsville, AL 35812, USA; <sup>ay</sup>JAXA, Ibaraki 305-8505, Japan; <sup>az</sup>Department of Physics, Nara Women’s University, Nara 630-8506, Japan; <sup>ba</sup>Columbia Astrophysics Laboratory, Department of Astronomy, Columbia University, New York, NY 10027, USA; <sup>bb</sup>European Space Agency (ESA) European Space Astronomy Centre (ESAC), Madrid, Spain; <sup>bc</sup>Department of physics and Astronomy, University of Manitoba, Winnipeg, MB R3T 2N2, Canada; <sup>bd</sup>Department of Physics, Saitama University, Saitama 338-8570, Japan; <sup>be</sup>Faculty of Social and Information Sciences, Nihon Fukushi University, Aichi 475-0012, Japan;

## ABSTRACT

The joint JAXA/NASA ASTRO-H mission is the sixth in a series of highly successful X-ray missions initiated by the Institute of Space and Astronautical Science (ISAS). ASTRO-H will investigate the physics of the high-energy universe via a suite of four instruments, covering a very wide energy range, from 0.3 keV to 600 keV. These instruments include a high-resolution, high-throughput spectrometer sensitive over 0.3–12 keV with high spectral resolution of  $\Delta E \leq 7$  eV, enabled by a micro-calorimeter array located in the focal plane of thin-foil X-ray optics; hard X-ray imaging spectrometers covering 5–80 keV, located in the focal plane of multilayer-coated, focusing hard X-ray mirrors; a wide-field imaging spectrometer sensitive over 0.4–12 keV, with an X-ray CCD camera in the focal plane of a soft X-ray telescope; and a non-focusing Compton-camera type soft gamma-ray detector, sensitive in the 40–600 keV band. The simultaneous broad bandpass, coupled with high spectral resolution, will enable the pursuit of a wide variety of important science themes.

**Keywords:** X-ray, Hard X-ray, Gamma-ray, X-ray Astronomy, Gamma-ray Astronomy, micro-calorimeter

## 1. INTRODUCTION

ASTRO-H, which was formerly called NeXT, is an international X-ray satellite that Japan plans to launch with the H-II A rocket in 2014.<sup>1–6</sup> NASA has selected the US participation in ASTRO-H as a Mission of Opportunity in the Exploration Program. Under this program, the NASA/Goddard Space Flight Center collaborates with ISAS/JAXA on the implementation of an X-ray micro-calorimeter and soft X-ray telescopes (SXS Proposal NASA/GSFC, 2007).<sup>7</sup> Other international members are from Stanford University, SRON, Geneva University, CEA/DSM/IRFU, CSA and ESA. In early 2009, NASA, ESA and JAXA have selected science advisors to provide scientific guidance to the ASTRO-H project relative to the design/development and operation phases of the mission. The ESA contribution to the ASTRO-H Mission includes the procurement of payload hardware elements which enhance the scientific capability of the mission.

The history and evolution of the Universe can be described as a process in which structures of different scales such as stars, galaxies, and clusters of galaxies are formed. In some cases, during this process, the matter and energy concentrate to an extreme degree in the form of black holes and neutron stars. It is a mystery of Nature why and how the overwhelming diversity over orders of magnitude in spatial and density scales has been produced in the Universe following an expansion from a nearly uniform state. One of the best probes of this process are clusters of galaxies, the largest astronomical objects in the Universe. Observing

---

ASTRO-H Web site: <http://ASTRO-H.isas.jaxa.jp/index.html.en>



Figure 1. Schematic view of the ASTRO-H satellite. The total mass at launch will be  $\sim 2700$  kg. ASTRO-H will be launched into a circular orbit with altitude of 500 – 600 km, and inclination of  $\sim 31$  degrees.

Table 1. ASTRO-H Mission

Launch site	Tanegashima Space Center, Japan
Launch vehicle	JAXA H-IIA rocket
Orbit Altitude	$\sim 550$ km
Orbit Type	Approximate circular orbit
Orbit Inclination	$\sim 31$ degrees
Orbit Period	96 minutes
Total Length	14 m
Mass	$\sim 2.7$ metric ton
Power	$< 3500$ W
Telemetry Rate	8 Mbps (X-band QPSK)
Recording Capacity	12 Gbits at EOL
Mission life	$> 3$ years

clusters of galaxies and revealing their history will lead to an understanding of how the largest structures form and evolve in the Universe. Equally important is studying how supermassive black holes form and develop, and what a role they play in forming galaxies and clusters of galaxies.

The X-ray band is capable of probing extreme environments of the Universe such as those near black holes or the surface of neutron stars, as well as observing exclusively the emission from high-temperature gas and selectively the emission from accelerated electrons. In recent years, Chandra, XMM-Newton, Suzaku and other X-ray missions have made great advances in X-ray Astronomy. We have obtained knowledge that has revolutionized our understanding of the high energy Universe and we have learned that phenomena observed in the X-ray band are deeply connected to those observed in other wavelengths from radio to  $\gamma$ -rays.

In order to revolutionize X-ray astronomy even further, the ASTRO-H mission is equipped with a suite of sensitive instruments with the highest energy resolution ever achieved at  $E > 3$  keV and a wide energy range spanning four decades in energy from soft X-rays to gamma-rays (Fig. 1). This instrumental suite will provide the best sensitivity ever achieved for spectroscopy in the 1–600keV band. The mission aims to understand the dynamics of the Universe in general, and study compact regions of high matter and energy

concentration allowing probe of production of energetic particles, which are far from the thermal equilibrium.

## 2. SCIENCE REQUIREMENTS

ASTRO-H is advancing the technologies developed through a series of highly successful X-ray missions initiated in ISAS, beginning with the launch of the Hakucho mission in 1979 through to the currently operating Suzaku mission. The prime scientific goal for ASTRO-H is to address a number of fundamental questions in contemporary astrophysics, as listed below.

### Scientific Goals and Objectives

#### Revealing the large-scale structure of the Universe and its evolution

- ASTRO-H will observe clusters of galaxies, the largest bound structures in the Universe, with the aim to reveal the interplay between the thermal energy of the intracluster medium and the kinetic energy of sub-clusters, from which clusters form; measure the non-thermal energy and chemical composition; and to directly trace the dynamic evolution of clusters of galaxies.
- ASTRO-H will observe distant supermassive black holes hidden by thick intervening material with 100 times higher sensitivity than the currently operating Suzaku, and will study their evolution and a role they play in galaxy formation.

#### Understanding the extreme conditions in the Universe

- ASTRO-H will measure the motion of matter very close to black holes with the aim to sense the gravitational distortion of space to understand the structure of relativistic space-time and to study the physics of the accretion process.

#### Exploring the diverse phenomena of the non-thermal Universe

- ASTRO-H will derive the physical conditions of the sites where high energy cosmic ray particles gain energy and will elucidate the processes by which gravity, collisions, and stellar explosions energize those cosmic rays.

#### Elucidating dark matter and dark energy

- ASTRO-H will map the distribution of dark matter in clusters of galaxies and will determine the total mass of galaxy clusters at different distances (and thus at different ages), and will study the role of dark matter and dark energy in the evolution of these systems.

In order to achieve the cutting-edge scientific goals described above, ASTRO-H is designed with the most advanced technologies. With an unprecedented spectroscopic capability and a wide-band energy coverage, ASTRO-H will measure the motion of hot gas, depicting the dynamic nature of the evolution of the Universe. These measurements will be the key in the great pursuit to understand the origin of the dark matter filling the Universe.

## 3. SPACECRAFT AND INSTRUMENTS

The ASTRO-H X-ray observatory will consist of four focusing telescopes mounted on a fixed optical bench (FOB). Two of the four telescopes are Soft X-ray Telescopes (SXTs) and they have a 5.6 m focal length (Fig. 2). They will focus medium-energy X-rays ( $E \sim 0.3\text{-}12\text{ keV}$ ) onto focal plane detectors mounted on the base plate of the FOB. One SXT will point to a micro-calorimeter spectrometer array with excellent energy resolution of  $\leq 7\text{ eV}$ , and the other SXT will point to a large-area CCD array. The other two telescopes are Hard X-ray Telescopes (HXTs) capable of focusing high-energy X-rays ( $E = 5\text{-}80\text{ keV}$ ). The focal length of the HXTs is 12 m. The Hard X-ray Imaging detectors (HXIs) are mounted at the end of a 6 m extendable optical bench (EOB) that is stowed to fit in the launch fairing and deployed once in orbit. In order to extend

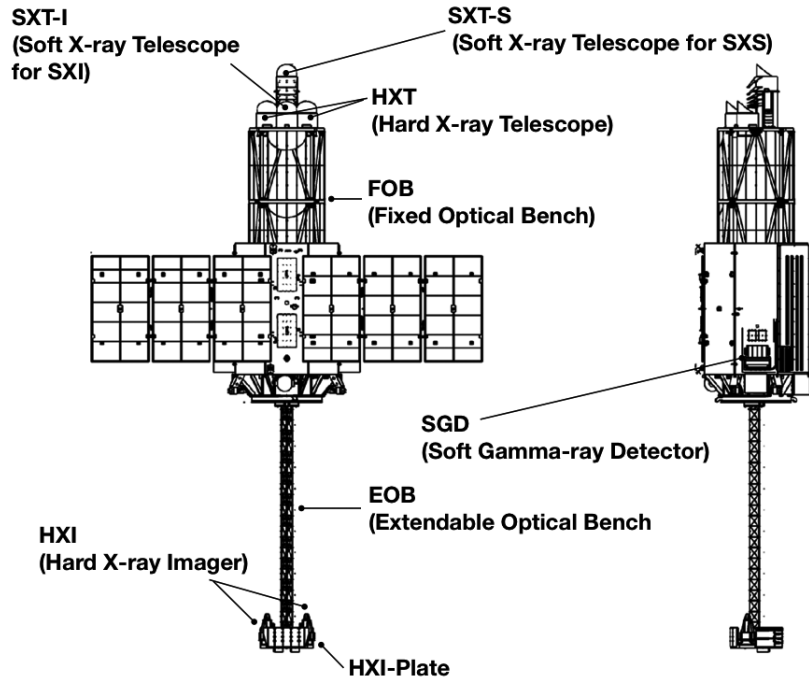


Figure 2. Schematic view of the ASTRO-H satellite.

the energy coverage to the soft  $\gamma$ -ray region up to 600 keV, the Soft Gamma-ray Detector (SGD) will be implemented as a non-focusing detector. Two SGD detectors, each consisting of three units will be mounted separately on two sides of the satellite. With these instruments, ASTRO-H will cover the entire bandpass between 0.3 keV and 600 keV. The key parameters of those instruments based on the base-line design are summarized in Table. 2.

The lightweight design of the EOB renders it to be vulnerable to distortions from thermal fluctuations in low-Earth orbit (LEO) and spacecraft attitude manoeuvres. Over the long exposures associated with X-ray observing, such fluctuations might impair HXI image quality unless a compensation technique is employed. To provide the required corrections, the Canadian contribution to the the ASTRO-H project is a laser metrology system (the Canadian ASTRO-H Metrology System, CAMS) that will measure displacement in the alignment of the HXT optical path. The CAMS consist of a laser and detector module (CAMS-LD) located on the top plate of the FOB, and a passive target module (CAMS-T) consisting of a retroreflector (corner cube mirror) mounted on the EOB detector plate.<sup>8</sup>

In the following sections, these instruments are briefly described. Detailed descriptions of the instruments and their current status are available in other papers in these proceedings.<sup>9-15</sup>

### 3.1 Soft X-ray Spectrometer System

The soft X-ray Spectrometer (SXS) consists of the Soft X-ray Telescope (SXT), the X-ray Calorimeter Spectrometer (XCS) and the cooling system.<sup>16,17</sup> The XCS is a 36-pixel system with an energy resolution of  $\leq 7$  eV between 0.3–12 keV (Fig. 3). The array design for the SXS is basically the same as that for the Suzaku/XRS, but has larger pixel pitch and absorber size. HgTe absorbers are attached to ion-implanted Si thermistors formed on suspended Si micro-beams. The array has  $814 \mu\text{m}$  pixels on an  $832 \mu\text{m}$  pitch and was manufactured during the Suzaku/XRS program along with arrays with smaller pixel size as an option for a larger field of view. For ASTRO-H, the longer focal length of the SXS (5.6 m vs. 4.5 m for Suzaku) necessitated the use of these larger arrays to maintain a FOV of at least  $2.9 \times 2.9$  arcminutes. The 8.5-micron-thick absorbers were fabricated by EPIR Corporation and diced using reactive ion etching. These absorbers provide high quantum efficiency across the 0.3–12 keV band. Despite the larger pixel size

Table 2. Key parameters of the ASTRO-H payload

Parameter	Hard X-ray Imager (HXI)	Soft X-ray Spectrometer (SXS)	Soft X-ray Imager (SXI)	Soft $\gamma$ -ray Detector (SGD)
Detector technology	Si/CdTe cross-strips	micro calorimeter	X-ray CCD	Si/CdTe Compton Camera
Focal length	12 m	5.6 m	5.6 m	–
Effective area	300 cm <sup>2</sup> @30 keV	210 cm <sup>2</sup> @6 keV 160 cm <sup>2</sup> @ 1 keV	360 cm <sup>2</sup> @6 keV	>20 cm <sup>2</sup> @100 keV Compton Mode
Energy range	5 –80 keV	0.3 – 12 keV	0.5 – 12 keV	40 – 600 keV
Energy resolution (FWHM)	2 keV (@60 keV)	< 7 eV (@6 keV)	< 200 eV (@6 keV)	< 4 keV (@60 keV)
Angular resolution	<1.7 arcmin	<1.3 arcmin	<1.3 arcmin	–
Effective Field of View	$\sim 9 \times 9$ arcmin <sup>2</sup>	$\sim 3 \times 3$ arcmin <sup>2</sup>	$\sim 38 \times 38$ arcmin <sup>2</sup>	$0.6 \times 0.6$ deg <sup>2</sup> (< 150 keV)
Time resolution	25.6 $\mu$ s	5 $\mu$ s	4 sec/0.1 sec	25.6 $\mu$ s
Operating temperature	–20°C	50 mK	–120°C	–20°C



Figure 3. The SXS engineering model detector assembly. At the center of the assembly is the x-ray calorimeter housing. This is suspended from the outer structure using Kevlar, and electrical connections to the housing are made using tensioned wires to reduce the sensitivity to microphonics. At the center of the calorimeter housing is an aluminum/polyimide blocking filter and a <sup>55</sup>Fe calibration source used to illuminate a dedicated calibration pixel for monitoring the absolute gain. The overall assembly is about 12.7 cm in diameter.

for the SXS (factor of 1.7 in volume), the energy resolution is substantially improved from  $\sim 6$  eV to  $\sim 4$  eV (FWHM) (Fig. 4). The main reasons for this are that EPIR developed a process to produce HgTe with lower specific heat and that the operating temperature of the instrument has been lowered from 60 mK to 50 mK.<sup>25</sup>

With a 5.6-m focal length, the 0.83 mm pixel pitch corresponds to 0.51 arcmin, giving the array a field of view of 3.05 arcmin on a side. The detector assembly provides electrical, thermal, and mechanical interfaces between the detectors (calorimeter array and anti-coincidence particle detector) and the rest of the instrument. The SXT for the XCS is an upgraded version of the Suzaku X-ray telescope with improved angular resolution and larger collecting area.<sup>18,19</sup> The SXS effective area at 6 keV will be at least 210 cm<sup>2</sup>,

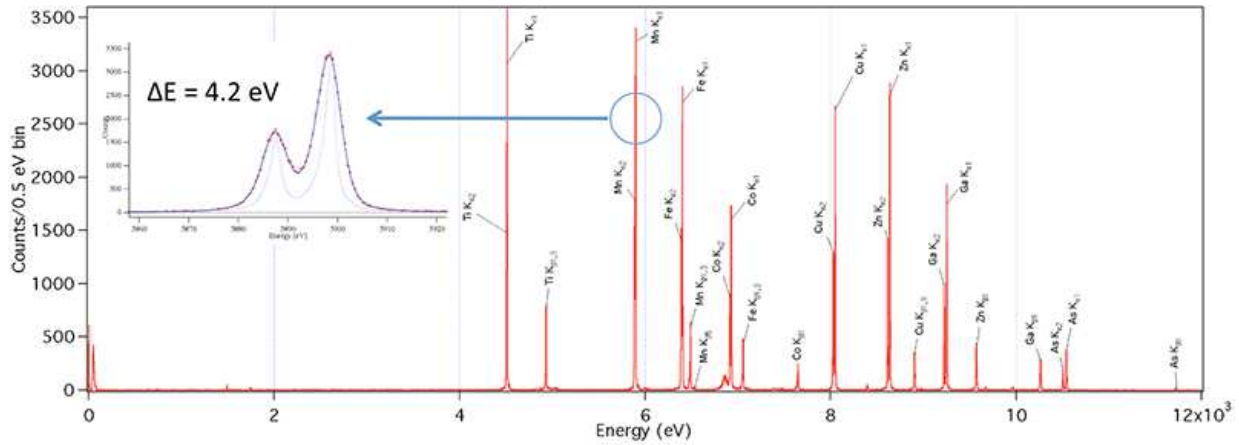


Figure 4. Laboratory X-ray spectrum obtained with the Astro-H Soft X-Ray Spectrometer engineering model detector assembly. The spectrum shows the enormous spectral dynamic range that can be obtained. The spectral resolution is 4.2 eV over the entire array, and is achieved over the full energy range where astrophysically abundant atomic transitions will be detected (less than about 8 keV), providing a resolving power of about about 1400 at 6 keV. The required resolution is 7 eV.

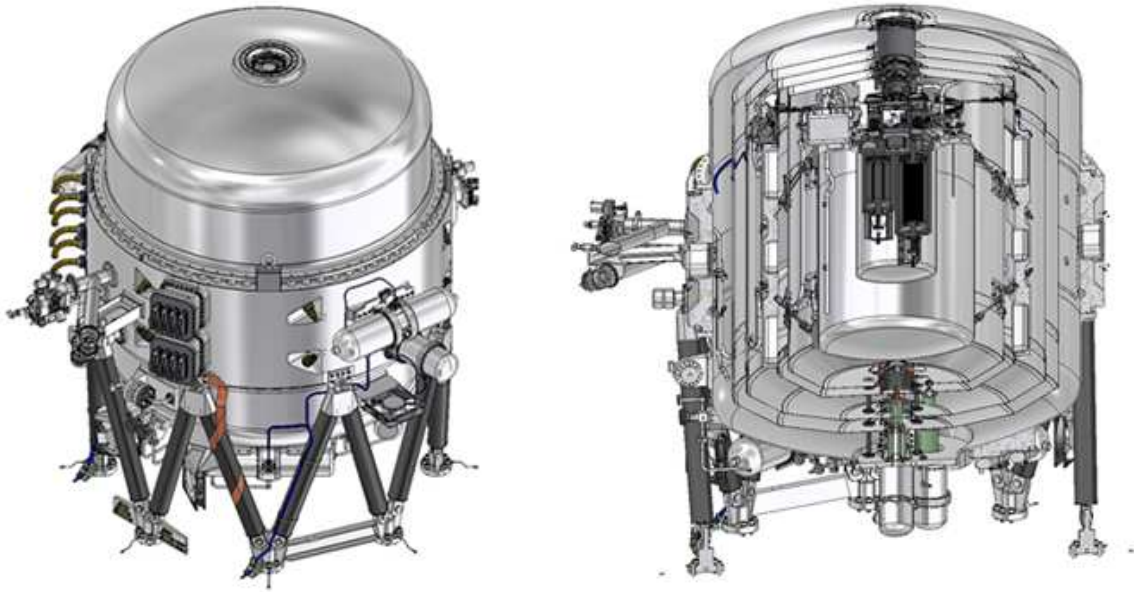


Figure 5. Outlook and cross sectional view of the SXS dewar. The outer shell of the dewar is 950 mm in diameter.

a 60 % increase over the Suzaku XRS, while at 1 keV the SXS has 160 cm<sup>2</sup>, a 20 % increase.

The XCS cooling system must cool the array to 50 mK with sufficient duty cycle to fulfill the SXS scientific objectives: this requires extremely low heat loads. To achieve the necessary gain stability and energy resolution, the cooling system must regulate the detector temperature to within 2  $\mu$ K rms for at least 24 hours per cycle.<sup>10,20</sup> From the detector stage to room temperature, the cooling chain is composed of a 3-stage Adiabatic Demagnetization Refrigerator (ADR), superfluid liquid <sup>4</sup>He (hereafter LHe), a <sup>4</sup>He Joule-Thomson (JT) cryocooler, and 2-stage Stirling cryocoolers (Fig. 5.) An ADR has been adopted because it readily meets the requirements for detector temperature, stability, recycle time, reliability in the space environment, and previous flight heritage.<sup>21</sup> The design of Stirling cryocoolers is based on coolers developed for space-flight missions in Japan (Suzaku, AKARI, and the SMILES instrument deployed on the ISS<sup>22</sup>) that have achieved an excellent performance with respect to cooling power, efficiency, long life and mass. 30



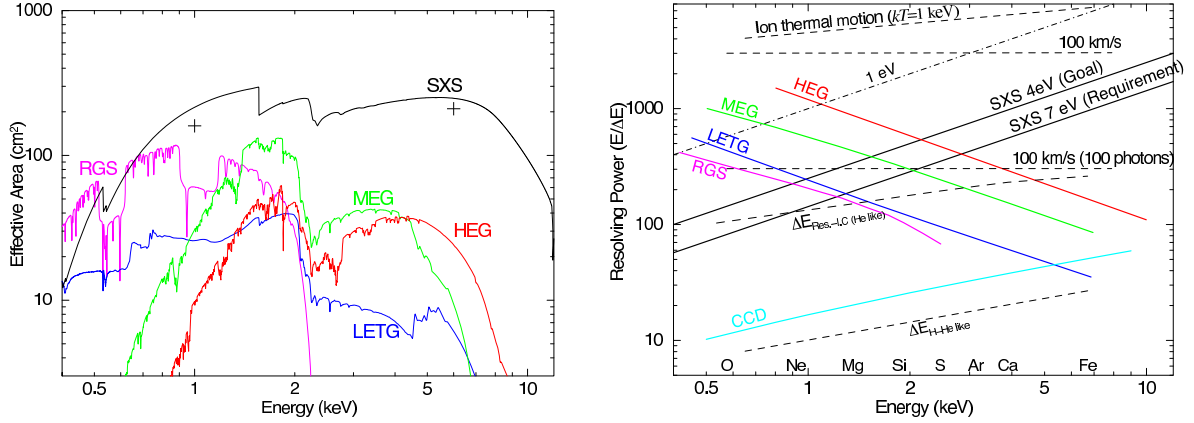


Figure 6. (a) Effective areas of high-resolution X-ray spectroscopy missions as functions of X-ray energy. The curve for the ASTRO-H SXS is the present best estimate for a point source. The two crosses show the mission requirements at specific energies. The XMM-Newton RGS effective area is the summation of first order spectra of the two instruments (RGS-1 and RGS-2). The effective areas of the LETG, MEG and HEG onboard Chandra are summations of the first order dispersions in  $\pm$  directions. (b) Resolving power of the ASTRO-H SXS as a function of X-ray energy for the two cases, 4 eV resolution (goal) and 7 eV (requirement). The resolving power of high resolution instruments onboard Chandra and XMM-Newton and typical resolving power of X-ray CCD cameras are also shown for comparison.<sup>16</sup>

L of LHe is used as a heat-sink for the 2-stage ADR. To reduce the parasitic heat load on the He tank, a  $^4\text{He}$  JT cryocooler is used to cool a 4 K shield. To achieve redundancy for failure (unexpected loss) of LHe, another ADR (3rd stage ADR) is used between the He tank and the JT cryocooler, with two heat-switches on both sides. This ADR is operated if LHe is lost, to cool down the 1 K shield (He tank). A series of five blocking filters shield the calorimeter array from UV and longer wavelength radiation. The aluminized polyimide filters are similar to those successfully used on Suzaku.

In combination with a high throughput X-ray telescope, the SXS improves on the Chandra and XMM-Newton grating spectrometers in two important ways. At  $E > 2$  keV, SXS is both more sensitive and has higher resolution (Fig.6), especially in the Fe K band where SXS has 10 times larger the collecting area and much better energy resolution, giving a net improvement in sensitivity by a factor of 30 over Chandra. The broad bandpass of the SXS encompasses the critical inner-shell emission and absorption lines of Fe I-XXVI between 6.4 and 9.1 keV. Fe K lines provide particularly useful diagnostics because of their (1) strength, due to the high abundance and large fluorescent yield (30%), (2) spectral isolation from other lines, and (3) relative simplicity of the atomic physics. Fe K emission lines reveal conditions in plasmas with temperatures between  $10^7$  and  $10^8$  K, which are typical values for stellar accretion disks, SNRs, clusters of galaxies, and many stellar coronae. In cooler plasmas, Si, S, and Fe fluorescence and recombination occurs when an X-ray source illuminates nearby neutral material. Fe emission lines provide powerful diagnostics of non-equilibrium ionization due to inner shell K-shell transitions from Fe XVII-XXIV.<sup>27</sup>

The SXS uniquely performs high-resolution spectroscopy of extended sources. In contrast to a grating, the spectral resolution of the calorimeter is unaffected by source's angular size because it is non-dispersive. For all sources with angular extent larger than 30 arcsec, Chandra MEG energy resolution is degraded compared with that of a CCD; the energy resolution of the XMM-Newton RGS is similarly degraded for sources with angular extent  $\geq 25$  arcsec. SXS therefore makes possible high-resolution spectroscopy of sources inaccessible to current grating instruments.

In order to obtain a good performance for bright sources, a filter wheel (FW) assembly, which includes a wheel with selectable filters and a set of modulated X-ray sources, are provided by SRON and Univ. of Geneva. It will be used at a distance of 90 cm from the detector. The FW is able to rotate a suitable filter into the beam to optimize the quality of the data, depending on the source characteristics.<sup>15, 23</sup> In addition to the filters, a set of on-off-switchable X-ray calibration sources, using light sensitive photo-cathode, will be implemented. With these calibration sources, it is possible to calibrate the energy scale with a typical 1–2 eV accuracy, and will allow proper gain and linearity calibration of the detector in flight.

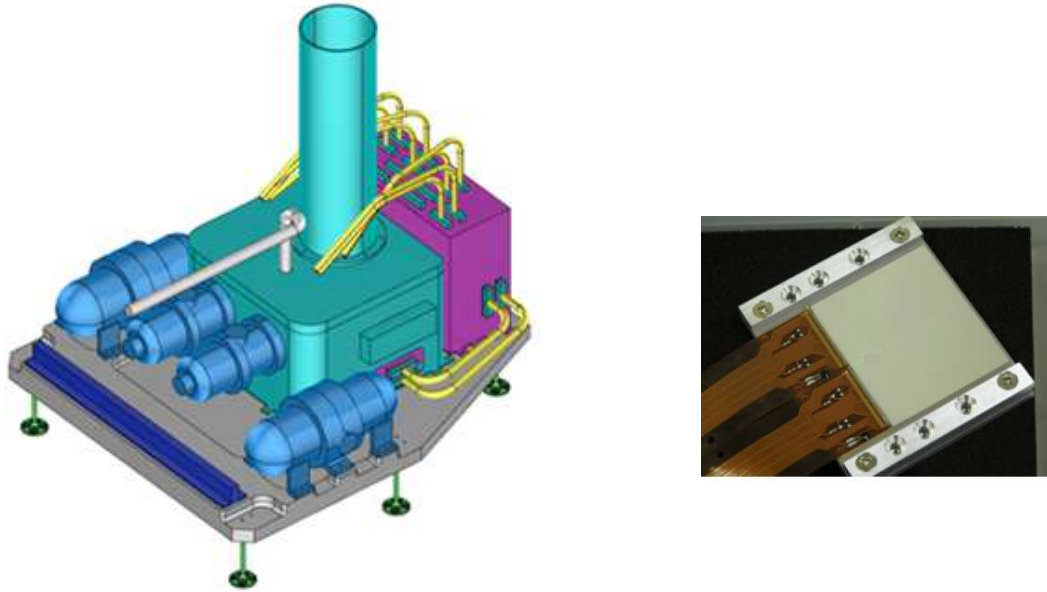


Figure 7. Schematic drawing of the Soft X-ray Imager and a picture of a prototype CCD chip.

### 3.2 Soft X-ray Imaging System

X-ray sensitive silicon charge-coupled devices (CCDs) are key detectors for X-ray astronomy. The low background and high energy resolution achieved with the XIS/Suzaku clearly show that the X-ray CCD can also play a very important role in the ASTRO-H mission. The soft X-ray imaging system will consist of an imaging mirror and a CCD camera, (Soft X-ray Telescope (SXT-I), Soft X-ray Imager (SXI)) and the cooling system.<sup>11,28–30</sup> Fig. 7 shows a schematic drawing of the SXI.

In order to cover the soft X-ray band below 12 keV, the SXI will use next generation Hamamatsu CCD chips with a thick depletion layer of 200  $\mu\text{m}$ , low noise, and almost no cosmetic defects. The SXI features a large FOV and covers a  $38 \times 38$  arcmin<sup>2</sup> region on the sky, complementing the smaller FOV of the SXS calorimeter (Fig. 8). A mechanical cooler ensures a long operational life at  $-120$  °C. The quantum efficiency is better than the one achieved in Suzaku XIS over the entire 0.3–12 keV bandpass. The imaging mirror has a 5.6-m focal length, and a diameter of 45 cm. The nominal aim point will be placed at the center of SXS field of view, which is 4.3 arcmin offset from the SXI center.

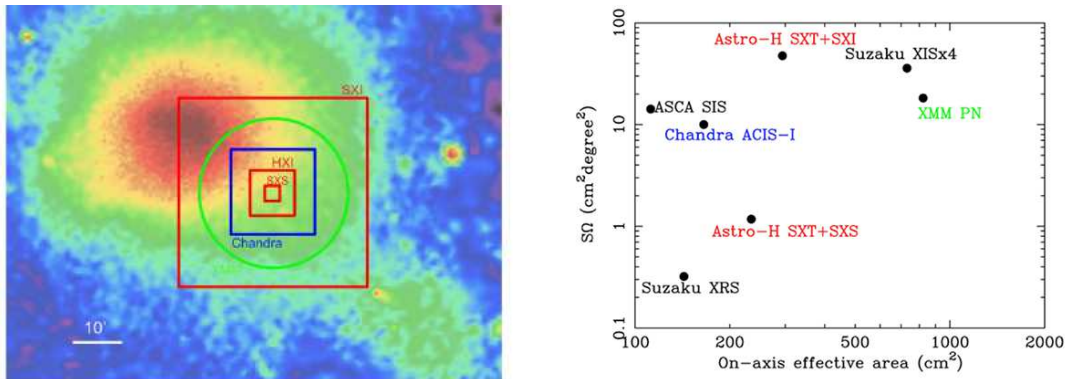


Figure 8. (left) Fields of view of the ASTRO-H instruments, SXS, SXI, HXI (the red boxes). Chandra ACIS-I and XMM are also shown for comparison. The background image is the Coma cluster taken with ROSAT (credit: ROSAT/MPE/S. L. Snowden). (right) Grasp vs on-axis effective area at 7 keV of SXT-I+SXI, SXT-S+SXS. Suzaku XIS, Chandra ACIS-I, XMM PN are also shown for comparison.

### 3.3 Hard X-ray Imaging System

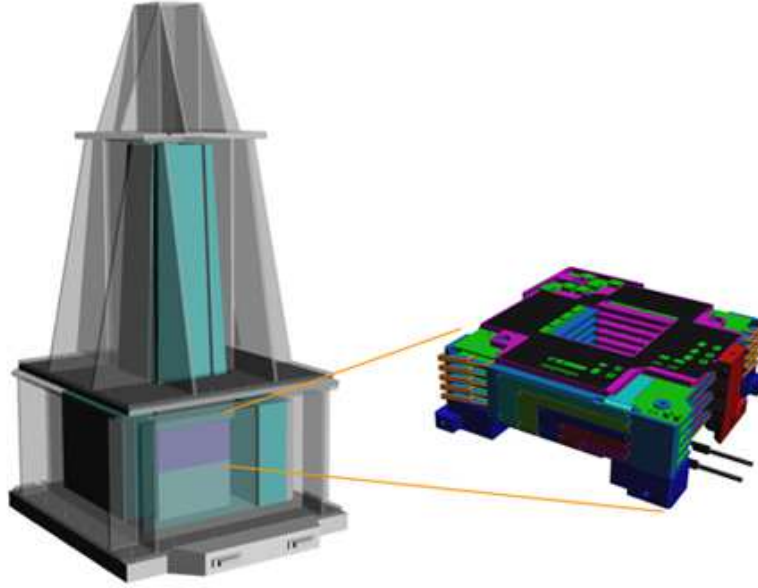


Figure 9. The Hard X-ray Imager. A stack of Si and CdTe double sided cross-strip detectors is mounted in a well-type BGO shield.

The hard X-ray imaging system onboard ASTRO-H consists of two identical mirror-detector pairs (HXT and HXI). The HXT has conical-foil mirrors with depth-graded multilayer reflecting surfaces that provide efficient reflection over 5–80 keV energy range.<sup>12,31,32</sup> The effective area of the HXT is maximized for a long focal length.

A depth-graded multilayer mirror reflects X-rays not only by total external reflection but also by the Bragg reflection. In order to obtain a high reflectivity up to 80 keV, the HXTs consist of a stack of multilayers with different sets of periodic length and number of layer pairs with a platinum/carbon coating. The technology of a hard X-ray focusing mirror has already been proven by the balloon programs InFOC $\mu$ S (2001, 2004),<sup>33,34</sup> HEFT (2004)<sup>35</sup> and SUMIT (2006)<sup>33</sup> and very recently with the NuSTAR satellite.<sup>36</sup>

Recent test of the first flight mirror have validated the HXT design, achieving a collecting area of 174 cm<sup>2</sup> at 30 keV for one telescope, with a focal length of 12 m.

The non-imaging instruments flown so far were essentially limited to studies of sources with 10–100 keV fluxes of  $>4 \times 10^{-12}$ – $10^{-11}$  erg cm<sup>-2</sup>s<sup>-1</sup>, at best. This limitation is due to the presence of high un-rejected backgrounds from particle events and Cosmic X-ray radiation, which increasingly dominate above 10 keV. Imaging, and especially focusing instruments have two tremendous advantages. Firstly, the volume of the focal plane detector can be made much smaller than for non-focusing instruments, thus reducing the absolute background level since the background flux generally scales with the size of the detector. Secondly, the residual background, often time-variable, can be measured simultaneously with the source, and can be reliably subtracted. For these reasons, a focusing hard X-ray telescope in conjunction with an imaging detector sensitive for hard X-ray photons is the appropriate choice to achieve a breakthrough in sensitivity for the field of high energy astronomy. In addition to the improvement of sensitivity, the HXI provides a true imaging capability which enable us to study spatial distributions of hard X-ray emission.

The HXI sensor consists of four layers of 0.5 mm thick Double-sided Silicon Strip Detectors (DSSD) and one layer of 0.75 mm thick CdTe imaging detector (Fig. 9).<sup>13,37–40</sup> In this configuration, soft X-ray photons below  $\sim 20$  keV are absorbed in the Si part (DSSD), while hard X-ray photons above  $\sim 20$  keV go through

the Si part and are detected by a newly developed CdTe double sided cross-strip detector. The low energy spectrum, obtained with Si, is less contaminated by the background due to activation in heavy material, such as Cd and Te. The DSSDs cover the energy below 30 keV while the CdTe strip detector covers the 20–80 keV band. Each DSSD has a size of  $3.2 \times 3.2 \text{ cm}^2$  and a thickness of 0.5 mm, resulting in 2 mm in total thickness, the same as that of the PIN detector of the HXD onboard Suzaku. A CdTe strip detector has a size of  $3.2 \times 3.2 \text{ cm}^2$  and a thickness of 0.75 mm. In addition to the increase of efficiency, the stack configuration and individual readout provide information on the interaction depth. This depth information is very useful to reduce the background in space applications, because we can expect that low energy X-rays interact in the upper layers and, therefore, it is possible to reject the low energy events detected in lower layers. Moreover, since the background rate scales with the detector volume, low energy events collected from the first few layers in the stacked detector have a high signal to background ratio, in comparison with events obtained from a monolithic detector with a thickness equal to the sum of all layers.

In the energy band above 10 keV, the number of photons from the source decreases and the detector background becomes the major limitations of its sensitivity. Since a significant fraction of the background events originate from interactions of the cosmic-ray with the detector structure, a tight active shield to reject cosmic-ray induced events is critical. Fast timing response of the silicon strip detector and CdTe strip detector allows us to place the entire detector inside a very deep well of an active shield made of BGO ( $\text{Bi}_4\text{Ge}_3\text{O}_{12}$ ) scintillators. The signal from the BGO shield is used to reject background events. The BGO scintillator crystal, with its high density and high absorbing power, is commonly used as a material for anti coincidence shields in recent hard X-ray/soft gamma-ray instruments, such as INTEGRAL and Suzaku/HXD. In ASTRO-H/HXI and SGD, a 3-4 cm thick BGO crystal is employed. With this thickness, it can not only tag the cosmic-rays, but also reduce the number of protons hitting the detector material (e.g., CdTe) by its passive shielding and hence it reduces the background.

### 3.4 Soft Gamma-ray Detector (SGD)

Highly sensitive observations in the energy range above the HXT/HXI bandpass are crucial to study the spectrum of X-rays arising from accelerated particles and black holes. In order to extend the energy coverage to the soft  $\gamma$ -ray region up to 600 keV, the Soft Gamma-ray Detector (SGD) will be implemented as a non-focusing detector onboard ASTRO-H.<sup>14,41</sup> The SGD measures soft  $\gamma$ -rays via reconstruction of the Compton scattering in the Compton camera, covering an energy range of 40 – 600 keV with sensitivity at 300 keV of more than 10 times that of the Suzaku Hard X-ray Detector. It outperforms previous soft- $\gamma$ -ray instruments in background rejection capability by adopting a new concept of narrow-FOV Compton telescope.<sup>42,43</sup>

In order to lower the background dramatically and thus to improve the sensitivity as compared to the HXD of Suzaku, the design combines a stack of Si and CdTe pixel detectors to form a Compton camera (Si/CdTe Compton Camera).<sup>44</sup> The telescope is then mounted inside the bottom of a well-type active shield. Above  $\sim 40$  keV, each valid event is required to interact twice in the stacked detector, once by Compton scattering in a stack of Si strip detectors, and then by photo-absorption in the CdTe part (Compton mode). Once the locations and energies of the two interactions are measured, the Compton kinematics allows the calculation of the energy and direction (as a cone in the sky) of the incident  $\gamma$ -ray. The major advantage of employing a narrow FOV is that the direction of incident  $\gamma$ -rays is constrained to be inside the FOV. If the Compton cone does not intercept the FOV, we can reject the event as background. Most of the background can be rejected by requiring this condition.<sup>42</sup>

As shown schematically in Fig. 10, the detector consists of 32 layers of 0.6 mm thick Si pad detectors and eight layers of CdTe pixellated detectors with a thickness of 0.75 mm. The sides are also surrounded by two layers of CdTe pixel detectors. The opening angle provided by the BGO shield is  $\sim 10$  degrees at 500 keV. As compared to the HXD, the shield part is made compact by adopting the newly developed avalanche photo-diode. An additional PCuSn collimator restricts the field of view of the telescope to  $30^\circ$  for photons below 100 keV to minimize the flux due to the Cosmic X-ray Background in the FOV. These modules are then arrayed to provide the required area.

The effective area of the SGD is  $>20 \text{ cm}^2$  at 100 keV in the Compton mode. It should be noted that when the Compton condition is not used, the stacked DSSD can be used as a standard photo-absorption

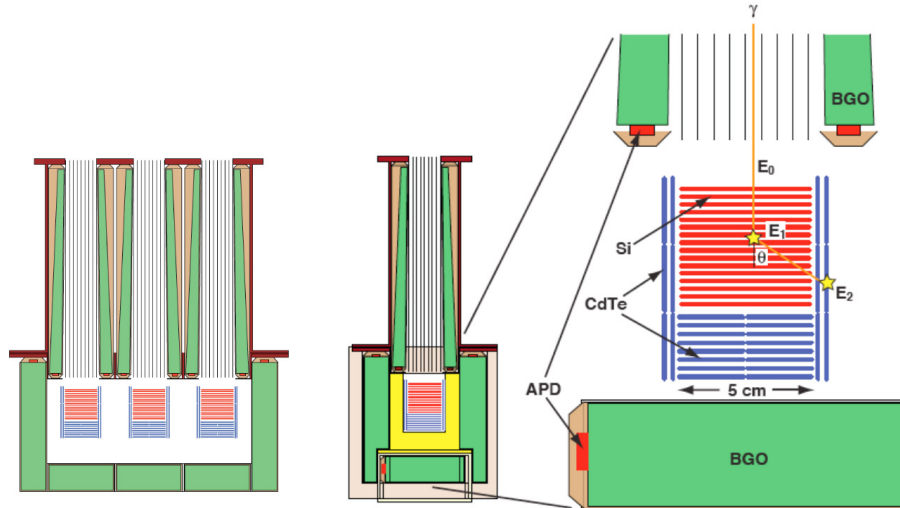


Figure 10. Conceptual drawing of an SGD Compton camera unit (green sections are the BGO anti-coincidence shields, red planes are the Si strip detectors in which the Compton scattering, occurs and the blue parts are the CdTe section in which the photons are absorbed).

type detector with the total thickness  $\sim 20$  mm of silicon. The detector then covers energies above 10 keV as a collimated-type  $\gamma$ -ray detector.

Since the scattering angle of gamma-rays can be measured via reconstruction of the Compton scattering in the Compton camera, the SGD is capable of measuring polarization of celestial sources brighter than a few  $\times 1/100$  of the Crab Nebula, polarized above  $\sim 10\%$ . This capability is expected to yield polarization measurements in several celestial objects, providing new insights into properties of soft gamma-ray emission processes.<sup>41,48</sup>

Last year, the technology behind the SGD was proved in measurements of the distribution of Cs-137 in the environment of Fukushima.<sup>46</sup> In addition to showing that the SGD technology works as designed ‘in the field’ the use of the Si/CdTe Compton Camera provided crucial information in understanding how the fall out from the 2011 nuclear accident was distributed.

#### 4. SCIENCE OPERATION

ASTRO-H is in many ways similar to Suzaku in terms of orbit, pointing, and tracking capabilities, although the mass is considerably larger (the total mass at launch will be 2700 kg, nearly double Suzaku’s 1700 kg). ASTRO-H will be launched into a circular orbit with altitude of 500–600 km, and inclination of 31 degrees. Science operations will be similar to those of Suzaku, with pointed observation of each target until the integrated observing time is accumulated, and then slewing to the next target. A typical observation will require a few  $\times 100$  ksec integrated exposure time. All instruments are co-aligned and will operate simultaneously. The current plan is to use the first three months for check-out and start the PV phase with observations proprietary to the ASTRO-H team. Guest observing time will start from 10 months after the launch. About 75% of the satellite time will be devoted to GO observations after the PV phase is completed. We are planning to implement key-project type observations in conjunction with the GO observation time.

#### 5. EXPECTED SCIENTIFIC PERFORMANCE

The spectroscopic capability of X-ray micro-calorimeters is unique in X-ray astronomy, since no other previously or currently operating spectrometers could achieve comparable high energy resolution, high quantum efficiency, and spectroscopy for spatially extended sources at the same time. Imaging spectroscopy with the Soft X-ray Spectrometer (SXS) of extended sources can reveal line broadening and Doppler shifts due

to turbulent or bulk velocities. This capability enables the determination of the level of turbulent pressure support in clusters, SNR ejecta dispersal patterns, the structure of AGN and starburst winds, and the spatially dependent abundance pattern in clusters and elliptical galaxies. The SXS can also measure the optical depths of resonance absorption lines, from which the degree and spatial extent of turbulence can be inferred. Additionally, the SXS can reveal the presence of relatively rare elements in SNRs and other sources through its high sensitivity to low equivalent width emission lines. The low SXS background ensures that the observations of almost all line-rich objects will be photon limited rather than background limited.

The imaging capabilities at high X-ray energies will open a new era in high spatial-resolution studies of astrophysical sources of non-thermal emission above 10 keV, probed simultaneously with lower energy imaging spectroscopy. This will enable us to track the evolution of active galaxies with accretion flows which are heavily obscured, in order to accurately assess their contribution to black hole growth over cosmological time scale. It will also uniquely allow mapping of the spatial extent of the hard X-ray emission in diffuse sources, thus tracing the sites of cosmic ray acceleration in structures ranging in size from megaparsecs, such as clusters of galaxies, down to parsecs, such as young supernova remnants.<sup>51–53</sup> Those studies will be complementary to the SXS measurements: observing the hard X-ray synchrotron emission will allow a study of the most energetic particles, thus revealing the details of particle acceleration mechanisms in supernova remnants, while the high resolution SXS data on the gas kinematics of the remnant will constrain the energy input into the accelerators.

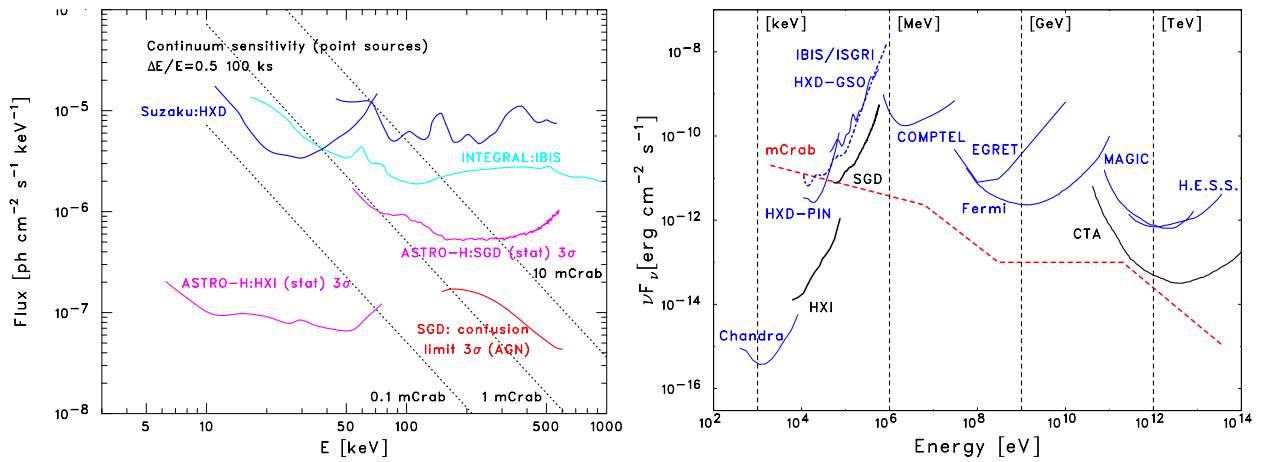


Figure 11. (left) The  $3\sigma$  sensitivity curves for the HXI and SGD onboard ASTRO-H for an isolated point source. (100 ks exposures and  $\Delta E/E = 0.5$ ) (right) Differential sensitivities of different X-ray and  $\gamma$ -ray instruments for an isolated point source.<sup>47</sup> Lines for the Chandra/ACIS-S, the Suzaku/HXD (PIN and GSO), the INTEGRAL/IBIS (from the 2009 IBIS Observer’s Manual), and the ASTRO-H/HXI,SGD are the  $3\sigma$  sensitivity curves for 100 ks exposures. A spectral bin with  $\Delta E/E = 1$  is assumed for Chandra and  $\Delta E/E = 0.5$  for the other instruments.

As shown in Figure 11, the sensitivity to be achieved by ASTRO-H (and similarly NuSTAR) is about two orders of magnitude improved compared to previous collimated or coded mask instruments that have operated in this energy band. This will bring a breakthrough in our understanding of hard X-ray spectra of celestial sources in general. With this sensitivity, 30 – 50% of the hard X-ray Cosmic Background will be resolved. This will enable us to track the evolution of active galaxies with accretion flows that are heavily obscured, in order to accurately assess their contribution to the Cosmic X-ray Background (i.e., black hole growth) over cosmic time. In addition, simultaneous observations of blazar-type active galaxies with Fermi-LAT and the TeV  $\gamma$ -ray telescopes are of vital importance to study particle acceleration in relativistic jets. An exciting and unique possibility is the detection of the polarization in hard X-rays by SGD during particularly strong flaring states of the brightest BL Lacs, like that of Mrk 501 in 1997 when the synchrotron continuum of the source extended up to the  $\gtrsim 100$  keV photon energy range.<sup>47, 48</sup>

In the following sections, we give a few examples of key science which will be addressed by ASTRO-H.

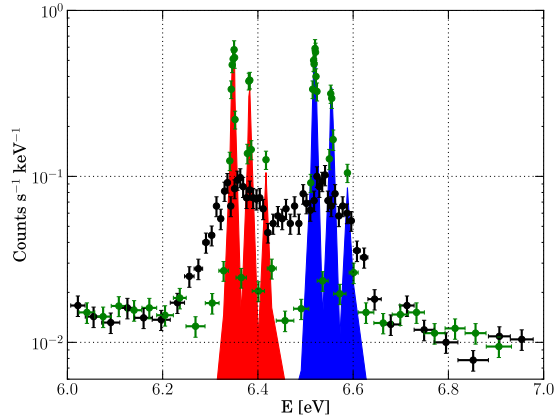


Figure 12. Simulated ASTRO-H SXS spectrum (black points) around the iron K-shell complex of Tycho’s SNR for an exposure of 100 ks.<sup>49</sup> For reference, a simulated spectrum with no thermal Doppler broadening is also shown (green points). Iron K lines from a blob that is receding are red-shaded, while lines from an approaching blob are blue-shaded.

## 5.1 Supernova Remnants

The high resolution X-ray spectroscopy provided by ASTRO-H will be particularly ground-breaking for supernova remnants (SNRs) because they are extended objects with rich emission-line spectra from a wide range of different elements (carbon through nickel). To determine the element abundances reliably, measurements of the relative strengths of a number of lines from each elemental species are required. Accurate element abundances provide constraints to test the explosion mechanisms of supernovae and to explore their environments. Gas motions of the rapidly expanding supernova ejecta and swept-up interstellar/circumstellar medium can also be measured by ASTRO-H via their Doppler shifts. Velocity measurements inferred from such Doppler shifts are needed to understand how SNRs evolve, based on their age and the detailed properties of the explosion, the ejecta, and ambient medium.

The excellent resolution of the ASTRO-H SXS offers an opportunity to measure the temperature of shocked iron ions in young SNR, a potential breakthrough in understanding the physics of shock heating. Figure 12 presents simulated spectra of SXS observations of the central portion of Tycho’s SNR. The spectrum shown with black points in Fig. 12 corresponds to the emission produced by two plasma blobs which were assumed to be receding and approaching us with  $\pm 4000 \text{ km s}^{-1}$  with the same parameters:<sup>50</sup> an iron temperature of  $kT_{\text{Fe}} = 3 \text{ MeV}$  (mass-proportional heating), an electron temperature of  $kT_e = 5 \text{ keV}$ , and an ionization parameter of  $\tau = 0.9 \times 10^{10} \text{ s cm}^{-3}$ . For a reference, a simulated spectrum with no thermal Doppler broadening is also shown (green points).<sup>47</sup>

Particle acceleration is receiving much attention at present, but the origin of cosmic rays is still unclear 100 years after their discovery. Young SNRs with shock speeds of several 1000 km/s are among the best candidates to accelerate cosmic rays up to energies around  $10^{15} \text{ eV}$  (the “knee” in the observed cosmic ray spectrum). The combination of ASTRO-H’s hard X-ray imaging capability and high spectral resolution will provide a unique insight into several crucial aspects of shock acceleration in SNRs such as the maximum energy of the accelerated particles, background conditions around the shock fronts, and the particle acceleration efficiency (See Fig. 13). High energy protons in SNR can be also studied with HXI through the detection of the synchrotron emission produced by secondary pair generated at proton-proton collisions.

## 5.2 A Census of Obscured Active Galactic Nuclei

Recent observations imply the existence of a large number of Active Galactic Nuclei (AGN) that are heavily obscured by the gas and dust surrounding their supermassive black holes.<sup>54,55</sup> Some of those are identified as a new type of AGN, so deeply buried in dense gas that they show little emission in the soft X-ray

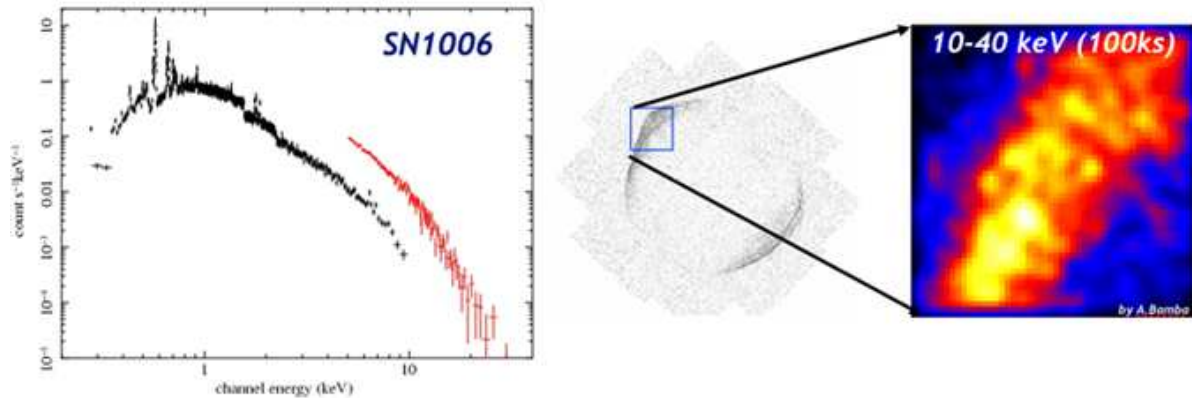


Figure 13. (left) Simulated spectra for 100 ks SXS observation of SN1006 with SXS and HXI. (right) Image expected from the combination of HXT and HXI.

or visible/ultraviolet light. While this has made such objects extremely difficult to detect and observe, this highly obscured activity may in fact represent the dominant phase of the supermassive black hole growth.<sup>56</sup> Understanding this phase is thus crucial for a proper understanding of the correlated evolution of supermassive black hole and their host galaxies. As shown in Fig. 12, the high sensitivity for hard X-rays provided by HXI allows precise spectral studies of even very obscured AGN. ASTRO-H will provide us with a large AGN sample to pursue systematic studies of the true AGN population, unbiased by obscuration effects and extending to far higher redshifts than current hard X-ray-selected samples,<sup>57</sup> allowing us to measure the co-evolution of supermassive black holes with their host galaxies.

By assuming a background level of  $\sim 1 \times 10^{-4}$  counts/s/cm<sup>2</sup>/keV, in which the non-X-ray background is dominant, the source detection limit in 1 Msec in the 10 – 80 keV band is roughly  $10^{-14}$  erg cm<sup>-2</sup> s<sup>-1</sup> (for a power-law spectrum with a photon index of 2). This is about two orders of magnitude better than previous instrumentation, and thus will result in a breakthrough in our understanding of hard X-ray spectra. With this sensitivity, 30-50 % of hard X-ray Cosmic Background is expected to be resolved<sup>55</sup>. In addition to the imaging below 80 keV, the SGD will enable high sensitivity observations in the soft  $\gamma$ -ray range closely matching the sensitivity of the HXT/HXI combination. The extremely low background observations allowed by the new concept of a narrow-FOV Compton telescope adopted for the SGD will provide sensitive  $\gamma$ -ray spectra up to 600 keV, with moderate sensitivity for polarization measurements.

### 5.3 Black Hole Vicinities

ASTRO-H provides an unprecedented view of the motions and extreme physical conditions of matter near the event horizon. This will help us to unravel how black holes grow by accreting matter and simultaneously how they influence their environments via radiative and mechanical energy output in the form of the intense emission fields and powerful, often relativistic outflows of magnetized plasma that accompany the accretion process.

Gaseous winds driven from black hole disks can carry away a substantial fraction of the gas that would otherwise accrete onto the central black hole. Such winds are hot, and most easily detected in the Fe K band via absorption lines. As shown in Fig. 15, the superior resolution of SXS in the Fe K band enables the unambiguous detection of weak and narrow lines from a wind. We will be able to use these to precisely determine the radius at which the wind is launched and the mass outflow rate carried by it. This will give us strong constraints on the driving mechanism of the wind and its feedback on the accretion flow as well as the black hole’s environment.<sup>59</sup>

On the smallest scales, many active galactic nuclei (AGN) show signatures from the the innermost parts of their accretion disk in the form of broad “relativistic” Fe K emission lines. These broad lines were discovered using ASCA in the early 1990s and have been confirmed by XMM-Newton and Suzaku.<sup>60,61</sup>



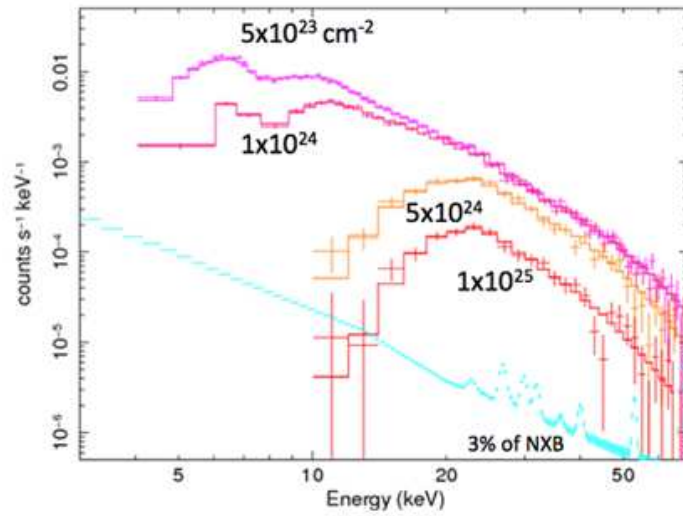


Figure 14. Simulated HXI spectra of heavily obscured AGN with different absorbing columns ( $N_H$ ) for an exposure of 100 ks. The continuum is assumed to be a power-law of photon index 1.9, with an intrinsic 2-10 keV flux of  $1 \times 10^{-11}$  erg/cm<sup>2</sup>/s (based on Swift J0601.9-8636<sup>54</sup>). The scattered component and Fe lines are not included. The light blue line represents the uncertainty in the background for a point source.

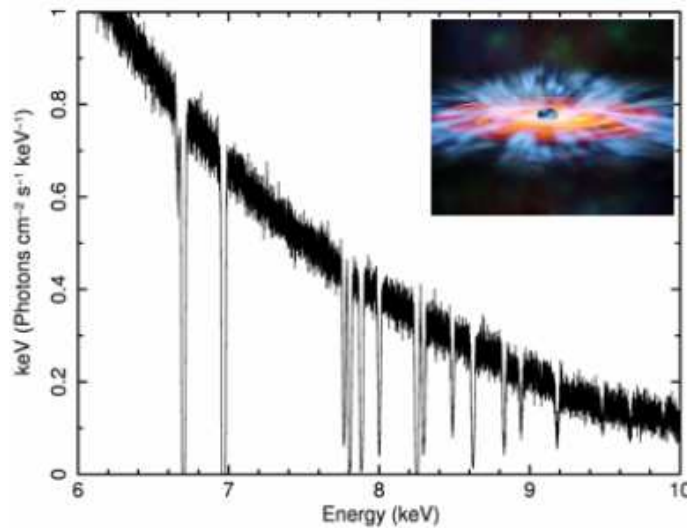


Figure 15. Simulated spectrum of the Galactic black hole candidate GRO J1655-40 for a 100 ks SXS observation,<sup>49</sup> based on a model that explains a prior Chandra observation. The dips in the spectrum are due to absorption from a highly ionized outflowing wind, comprised of atomic species from oxygen to nickel, that is driven by magnetic fields.<sup>58</sup>

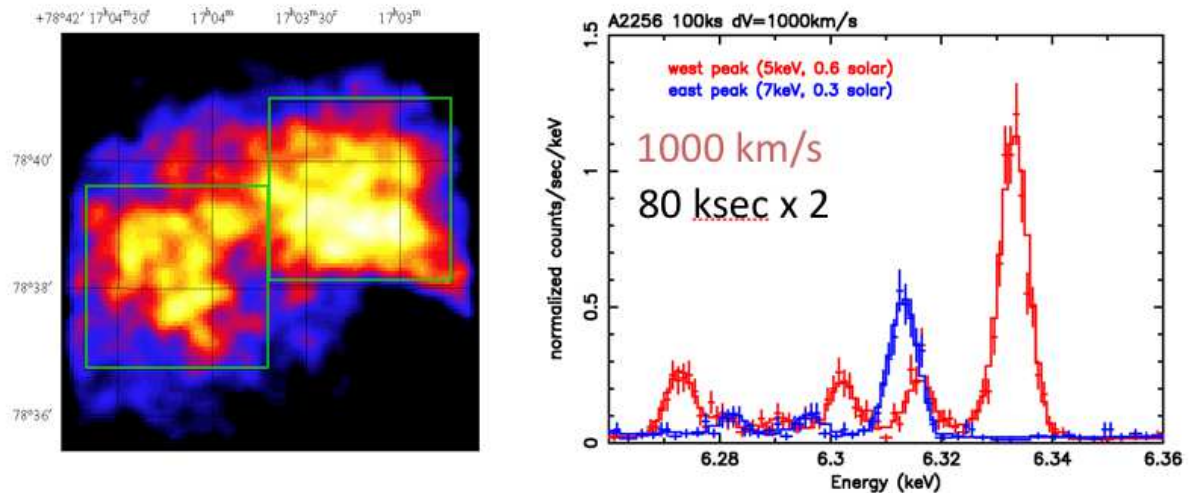


Figure 16. Simulated image and spectra of a merging cluster A2256 by assuming 1000 km/s difference of line of sight speed of hot gas in the cluster. The simulation is for 80 ksec each.

There is, however, a complex relationship between the Fe K line properties, the underlying continuum, and the signatures of cold and/or partially ionized material near the AGN. Precise measurements of the complex Fe K line and absorption components require high spectral resolution. The measurement of changes in the X-ray emission and absorption spectral features, on the orbital time scale of black holes in AGN, will enable characterization of the velocity field and ionization state of the plasma closest to the event horizon. The optically thick material that produces the broad fluorescent Fe K line also creates a Compton reflection “hump” peaking at  $E > 20$  keV detectable with hard X-ray and soft gamma-ray detectors, providing multiple insights into the physics of the disk. In order to understand the evolution of environments surrounding supermassive black holes, high signal-to-noise measurements of the broad lines of many AGN are needed up to, at least,  $z \sim 1$ . This requires high spectral resolution and bandpass extending to at least  $\sim 40$  keV. These observations will provide the first unbiased survey of broad Fe K line properties to  $z \sim 1$ . We will sample a few high- $z$ , high-luminosity AGN with adequate S/N and time resolution.

XMM-Newton and Suzaku spectra frequently show time-variable absorption and emission features in the 5–10 keV band. If these features are due to Fe, they represent gas moving at very high velocities with both red- and blue-shifted components from material presumably near the event horizon. CCD resolution is insufficient, and the required grating exposures are too long, to properly characterize the velocity field and ionization of this gas and determine whether it is from close to the black hole or from high velocity winds. SXS, in combination with HXI, provides a dramatic increase in sensitivity over Suzaku, enabling measurements that probe the geometry of the central regions of  $\sim 50$  AGNs on the orbital timescale of the Fe producing region (for an AGN with a  $3 \times 10^7 M_{\odot}$  black hole, this is  $\sim 60 GM/c^3 = 10$  ksec).

#### 5.4 Clusters of Galaxies

All studies of the total energy content (including that of non-thermal particles), aimed to draw a more complete picture of the high energy universe, require observations by *both* a spectrometer capable of measuring the bulk plasma velocities and/or turbulence with the resolution corresponding to the speed of a few  $\times 100$  km/s *and* an arc-min imaging system in the hard X-ray band, with sensitivity two-orders of magnitude better than previous missions (See Fig. 16 and Fig. 17). In clusters, X-ray emitting hot gas is trapped in the gravitational potential well, and shocks and/or turbulence are produced in this gas, as smaller substructures with their own hot gas halos fall into and merge with the dominant cluster. Large scale shocks can also be produced as gas from the intracluster medium falls into the gravitational potential of a cluster.

There is a strong synergy between the hard X-ray imaging data and the high resolution ( $\Delta E \leq 7$  eV) soft X-ray spectrometer: the kinematics of the gas, probed by the width and energy of the emission lines,

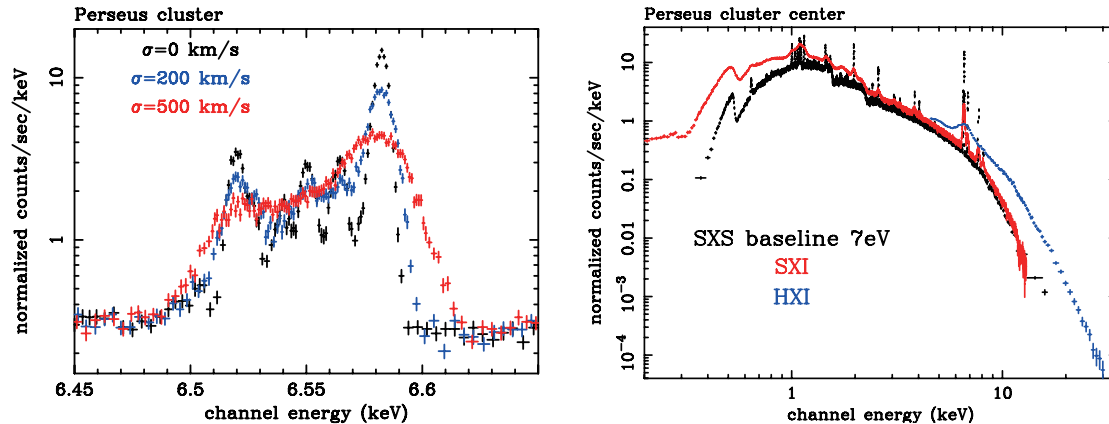


Figure 17. Simulated spectra for 100 ks ASTRO-H observations of Perseus Cluster. **(left)** SXS spectra around the iron K line complex. Line profiles assuming  $\sigma = 0, 200$  and  $500 \text{ km s}^{-1}$  turbulence. **(right)** SXS (black), SXI (red), and HXI (blue) spectra for hot plasma with a mixture of three different temperatures of 0.6, 2.6 and 6.1 keV ( $r < 2'$ ).<sup>6</sup>

constrains the energetics of the system,. The kinematics of the gas provides information about the bulk motion; the energy of this motion is in turn responsible for acceleration of particles to very high energies at shocks, which is in turn manifested via non-thermal emission processes, best studied via sensitive hard X-ray measurements.

Precision cosmology uses astronomical observations to determine the large-scale structure and content of the Universe. Studies of clusters of galaxies have provided independent measurements of the dark energy equation of state and strong evidence for the existence of dark matter. Using a variety of techniques (including the growth of structure, the baryonic fraction in clusters, and the Sunyaev-Zel'dovich effect) a well-constructed survey of clusters of galaxies, with the necessary supporting data,<sup>63</sup> can provide precise measurements of cosmological parameters, including the amount and properties of dark energy and dark matter. The key step is to connect observables (such as flux and temperature) to cluster masses. Currently, large area cluster surveys are being carried out using the Sunyaev-Zel'dovich Effect by the Atacama Cosmology Telescope, Planck, and the South Pole Telescope, to be joined in the near future by the eROSITA X-ray mission. To reduce the systematic uncertainties on the masses inferred from the coarser data from these surveys, a training set of precise cluster masses must be obtained. Measurements of the bulk motion of clusters of galaxies and amounts of non-thermal energies going to cosmic-ray acceleration could reduce the "... substantial uncertainties in the baryonic physics which prevents their use at a high level of precision at the present time" (Dark Energy Task Force<sup>64</sup>). Line diagnostics with energy resolution of  $\Delta E \leq 7 \text{ eV}$  greatly reduce the uncertainties in the baryonic physics by determining the velocity field, any deviations from thermal equilibrium, and an accurate temperature for each cluster. Information about the non-thermal particle content of clusters can be determined via measurements of their Compton upscattering of the CMB: this is best studied via hard X-ray imaging, providing additional clues about the physical state of the cluster gas.

## 6. SUMMARY

The ASTRO-H mission objectives are: to determine the evolution of yet-unknown obscured supermassive black holes (SMBHs) in Active Galactic Nuclei (AGN); to trace the growth history of the largest structures in the Universe; to trace the chemical evolution of the universe; to probe feedback from the growth of supermassive black holes onto their galaxy and cluster environments; to provide insights into the behavior of material in extreme gravitational fields; to determine the spin of black holes and the equation of state of neutron stars; to trace particle acceleration structures in clusters of galaxies and SNRs; and to investigate the detailed physics of astrophysical jets.

ASTRO-H will open a completely new field of spatial studies of non-thermal emission across a broad range of energies extending well above 10 keV with hard X-ray telescopes and enable us to track the evolution of

active galaxies with accretion flows that are heavily obscured. It will also uniquely allow mapping of the spatial extent of the hard X-ray emission in diffuse sources, thus tracing the sites of particle acceleration in structures ranging in size from clusters of galaxies down to supernova remnants. At even higher energies, the sensitivity of the SGD will allow us for the first time to routinely detect and characterize the spectra of bright AGN above 100 keV.

The key properties of SXS onboard ASTRO-H are its high spectral resolution for both point and diffuse sources over a broad bandpass ( $\leq 7$  eV FWHM throughout the 0.3–12 keV band), high sensitivity (effective area of 160 cm<sup>2</sup> at 1 keV and 210 cm<sup>2</sup> at 7 keV), and low non-X-ray background ( $1.5 \times 10^{-3}$  cts s<sup>-1</sup>keV<sup>-1</sup>). These properties open up a full range of plasma diagnostics and kinematic studies of X-ray emitting gas for thousands of targets, both Galactic and extragalactic. SXS improves upon and complements the current generation of X-ray missions, including Chandra, XMM-Newton, Suzaku, Swift and NuSTAR.

### Acknowledgments

The authors are deeply grateful for on-going contributions provided by other members in the ASTRO-H team in Japan, the US, Europe and Canada.

### REFERENCES

- [1] NeXT Satellite Proposal, the NeXT working group, submitted to ISAS/JAXA (2005)
- [2] NeXT Satellite Proposal, the NeXT working group, submitted to ISAS/JAXA (2003)
- [3] H. Kunieda, “Hard X-ray Telescope Mission (NeXT)” , Proc. SPIE, **5488**, 187 (2004)
- [4] T. Takahashi, K. Mitsuda, & H. Kunieda, “The NeXT Mission” ,Proc. SPIE, **6266**, 62660D (2006)
- [5] T. Takahashi et al., “The NeXT Mission” , Proc. SPIE, **7011**, 70110O-1 (2008)
- [6] T. Takahashi, K. Mitsuda, R.L. Kelley et al., “The ASTRO-H Mission” , Proc. SPIE, **7732**, pp. 77320Z-77320Z-18 (2010)
- [7] SXS Proposal, “High Resolution X-ray Spectroscopy for the JAXA New Exploration X-ray Telescope” , NASA/GSFC, submitted to NASA (2007)
- [8] L. Gallo et al., “The Canadian Astro-H Metrology System” , Proc. SPIE, **8443**, this issue (2012)
- [9] T. Okajima et al. “The first measurement of the ASTRO-H soft x-ray telescope performance” , Proc. SPIE, **8443**, this issue (2012)
- [10] R. Fujimoto et al., “Design and performance demonstration of the cooling system for the Soft X-ray Spectrometer (SXS) onboard Astro-H” , Proc. SPIE, **8443** this issue (2012)
- [11] H. Tsunemi et al., “Soft x-ray imager (SXI) onboard ASTRO-H” , Proc. SPIE, **8443**, this issue (2012)
- [12] H. Awaki et al., “Current status of ASTRO-H hard x-ray telescopes (HXTs)” , Proc. SPIE, **8443**, this issue (2012)
- [13] M. Kokubun et al., “Hard x-ray imager (HXI) for the ASTRO-H Mission” , Proc. SPIE, **8443**, this issue (2012)
- [14] S. Watanabe et al., “Soft gamma-ray detector for the ASTRO-H Mission” , Proc. SPIE, **8443**, this issue (2012)
- [15] C. P. de Vries et al., “Calibration sources for the soft x-ray spectrometer instrument on ASTRO-H” , Proc. SPIE, **8443**, this issue (2012)
- [16] K. Mitsuda et al. “The high-resolution x-ray microcalorimeter spectrometer system for the SXS on ASTRO-H” , Proc. SPIE **7732**, pp. 773211-773211-10 (2010)
- [17] K. Mitsuda et al. “The X-ray micro calorimeter on the NeXT mission” , Proc. SPIE, **7011**, 701102K-1 (2008)
- [18] T. Okajima et al., “Soft x-ray mirrors onboard the NeXT satellite” , Proc. SPIE, **7011**, 85 (2008)
- [19] P. Serlemitsos et al., “Foil x-ray mirrors for astronomical observations: still an evolving technology” , Proc. SPIE **7732**, pp. 77320A-77320A-6 (2010)
- [20] R. Fujimoto et al., “Cooling system for the soft x-ray spectrometer (SXS) onboard ASTRO-H” , Proc. SPIE **7732**, pp. 77323H-77323H-7 (2010)

- [21] J. Shirron et al. “Design of a 3-stage ADR for the soft x-ray spectrometer instrument on the ASTRO-H mission”, Proc. SPIE **7732**, pp. 773212-773212-9 (2010)
- [22] K. Narasaki, et al., “Development of cryogenic system for SMILES”, Advances in Cryogenic Engineering, **49B**, pp.1785-1794 (2004)
- [23] C. de Vries et al., “Filters and calibration sources for the Soft X-ray Spectrometer (SXS) instrument on ASTRO-H”, Proc. SPIE **7732**, pp. 773213-773213-9 (2010)
- [24] R.L. Kelley et al., “Ion-implanted Silicon X-Ray Calorimeters: Present and Future”, J. Low Tem Phys., **151**, Nos. 1-2 (2008)
- [25] F. S. Porter and et al., “The detector subsystem for the SXS instrument on the ASTRO-H Observatory”, Proc. SPIE **7732**, pp. 77323J-77323J-13 (2010)
- [26] F. S. Porter and et al., “The Astro-H Soft X-ray Spectrometer (SXS) ”, AIP Conference proceedings **1185**, pp.91-94 (2009)
- [27] V. Decaux et al., “High Resolution Measurement of the  $K_{\alpha}$  Spectrum of Fe XXV-XXVIII: New Spectral Diagnostics of Nonequilibrium Astrophysical Plasmas,” ApJ. **482**, pp. 1076-1084 (1997)
- [28] H. Tsunemi et al., “The SXI: CCD camera onboard ASTRO-H”, Proc. SPIE **7732**, pp. 773210-773210-11 (2010)
- [29] T. G. Tsuru et al., “Soft X-ray Imager (SXI) onboard the NeXT satellite”, Proc. SPIE, **6266**, 62662I (2006)
- [30] H. Tsunemi et al., “The SXI: CCD camera onboard the NeXT mission”, Proc. SPIE, **7011**, 70110Q-1 (2008)
- [31] H. Kunieda, H. Awaki et al., “Hard X-ray Telescope to be onboard ASTRO-H”, Proc. SPIE **7732**, pp. 773214-773214-12 (2010)
- [32] Y. Ogasaka et al., “The NeXT x-ray telescope system: status update”, Proc. SPIE, **7011**, 70110P-1 (2008)
- [33] H. Kunieda et al., “Balloon-borne hard X-ray Imaging Observation of non-thermal phenomena”, Proc. SPIE, **6266**, 62660B (2006)
- [34] Y. Ogasaka et al., “Thin-foil multilayer-supermirror hard x-ray telescopes for InFOCUS/SUMIT balloon experiments and NeXT satellite program”, Proc. SPIE **6688**, 668803 (2007).
- [35] F. Harrison et al., “Development of the High-Energy Focusing Telescope (HEFT) Balloon Experiment,” Proc. SPIE, **4012**, 693 (2000)
- [36] F. A. Harrison et al., “The Nuclear Spectroscopic Telescope Array (NuSTAR),” Proc. SPIE, 2010, **7732**, pp. 77320S-77320S-8 (2010).
- [37] T. Takahashi et al., “Wide band X-ray Imager (WXI) and Soft Gamma-ray Detector (SGD) for the NeXT Mission,” Proc. SPIE, **5488**, p549-560 (2004)
- [38] M. Kokubun et al., “Hard x-ray imager for the ASTRO-H Mission”, Proc. SPIE **7732**, pp. 773215-773215-13 (2010)
- [39] K. Nakazawa et al., “Hard X-ray Imager for the NeXT Mission”, Proc. SPIE, **6266**, 62662H (2006)
- [40] M. Kokubun et al., “Hard X-ray imager (HXI) for the NeXT mission”, Proc. SPIE, **7011**, 70110R-1 (2008)
- [41] H. Tajima. et al., “Soft Gamma-ray Detector for the ASTRO-H Mission”, Proc. SPIE **7732**, pp. 773216-773216-17 (2010)
- [42] T. Takahashi, T. Kamae, and K. Makishima, “Future Hard X-ray and Gamma-ray Observations.” in *New Century of X-ray Astronomy*, ASP **251** 210 (2002)
- [43] T. Takahashi, K. Nakazawa, T. Kamae, H. Tajima, Y. Fukazawa, M. Nomachi, and M. Kokubun “High resolution CdTe detectors for the next generation multi-Compton gamma-ray telescope”, Proc. SPIE, **4851**, pp. 1228-1235 (2003)
- [44] T. Takahashi et al. “Hard X-ray and Gamma-Ray Detectors for the NeXT mission”, *New Astronomy Reviews*, 48, pp. 309-313 (2004)
- [45] T. Takahashi, K. Makishima, T. Kamae, “Future Hard X-ray and Gamma-ray Observations”, in *New Century of X-ray Astronomy*, Astronomical Society of Pacific, volume 251, 210-213 (2001)
- [46] JAXA press release ([http://www.jaxa.jp/press/2012/03/20120329\\_compton\\_e.html](http://www.jaxa.jp/press/2012/03/20120329_compton_e.html)) (2012)

- [47] T. Takahashi, Y. Uchiyama, L. Stawarz “Multiwavelength Astronomy and CTA: X-rays”, *Astroparticle Physics* in press(arXiv:1205.2423v1) (2012)
- [48] H. Tajima, T. Mitani, T. Tanaka, H. Nakamura, T. Nakamoto, K. Nakazawa, T. Takahashi, Y. Fukazawa, T. Kamae, M. Kokubun, G. Madejski, D. Marlow, M. Nomachi, E. do Couto e Silva, “Gamma-ray polarimetry with Compton Telescope,” *Proc. SPIE*,**5488**, pp. 561-571 (2004)
- [49] ASTRO-H Quick Reference [http://astro-h.isas.jaxa.jp/researchers/news/2010/1119\\_e.html](http://astro-h.isas.jaxa.jp/researchers/news/2010/1119_e.html)
- [50] A. Hayato, et al., “Expansion Velocity of Ejecta in Tycho’s Supernova Remnant Measured by Doppler Broadened X-ray Line Emission”, *ApJ* **725**, 894-903 (2010)
- [51] K. Koyama et al., “Evidence for Shock Acceleration of High-Energy Electrons in the Supernova Remnant SN:1006, ” *Nature*, **378**, 255 (1995)
- [52] Y. Uchiyama, F. Aharonian, T. Tanaka, T. Takahashi, Y. Maeda, “Extremely fast acceleration of cosmic rays in a supernova remnant,” *Nature*, **449**, 576 (2007)
- [53] F. A. Aharonian, F., *Very high energy cosmic gamma radiation: A crucial window on the extreme universe*, World Scientific (2004)
- [54] Y. Ueda et al., “Suzaku Observations of Active Galactic Nuclei Detected in the Swift BAT Survey: Discovery of a New Type of Buried Supermassive Black Holes”, *ApJ*, **664**, pp. L79-L82 (2007)
- [55] Y. Ueda et al., “Cosmological Evolution of the Hard X-Ray Active Galactic Nucleus Luminosity Function and the Origin of the Hard X-Ray Background”, *ApJ*, **598**, 886 (2003)
- [56] E. Treister, C.M. Urry, S.M. Virani, “The Space Density of Compton-Thick Active Galactic Nucleus and the X-Ray Background,” *ApJ*, **696**, 110 (2009)
- [57] D. Ballantyne, A. Draper, K. Madsen, J. Rigby, E. Treister, “Lifting the Veil on Obscured Accretion: Active Galactic Nuclei Number Counts and Survey Strategies for Imaging Hard x-ray Missions”, *ApJ*, **736**, 56 (2011)
- [58] J. Miller, “Relativistic X-Ray Lines from the Inner Accretion Disks Around Black Holes”, *ARAA*, **45**, pp.441-479 (2007)
- [59] A. Fabian, “Observational Evidence of AGN Feedback”, *ARAA* in press (arXiv:1204.4114) (2012)
- [60] Y. Tanaka, et al., “Gravitationally Redshifted Emission Implying an Accretion Disk and Massive Black-Hole in the Active Galaxy MCG:-6-30-15”, *Nature*, **375**, 659 (1995)
- [61] J.N. Reeves et al., “Revealing the High Energy Emission from the Obscured Seyfert Galaxy MCG-5-23-16 with Suzaku” ,*PASJ*, **59S**, 301 (2007)
- [62] M. Markevitch and A. Vikhlinin, “Shocks and cold fronts in galaxy clusters”, *Physics Reports*, **443** pp. 1-53 (2007)
- [63] D. Rapetti, S. Allen, A. Mantz, “The prospects for constraining dark energy with future X-ray cluster gas mass fraction measurements” ,. *MNRAS*, **388**, pp. 1265-1278 (2008)
- [64] A. Albrecht et al., “Report of the Dark Energy Task Force”, arXiv:astro-ph/0609591v1 (2006)